

# Dispersion of the Break Energy in the GRB Internal Shock Model

Katsuaki ASANO

*Department of Earth and Space Science, Osaka University, Toyonaka, Osaka 560-0043*  
*asano@vega.ess.sci.osaka-u.ac.jp*

and

Shiho KOBAYASHI

*Center for Gravitational Wave Physics, Pennsylvania State University,*  
*University Park, PA 16802, U.S.A.*  
*Department of Astronomy and Astrophysics, Pennsylvania State University,*  
*University Park, PA 16802, U.S.A.*  
*shiho@gravity.psu.edu*

(Received 2003 January 8; accepted 2003 March 19)

## Abstract

In order to investigate the dispersion of the spectral break energy in gamma-ray bursts, we simulate internal shocks, including effects of shell-splitting after shell collisions and the Thomson optical depth due to electron–positron pairs produced by synchrotron photons. We produce pseudo observational data and estimate the break energy. If the distribution of initial Lorentz factors of shells has only one peak, many pulses with a break energy much lower than the typical observed value should be detected, while the effect of the Thomson optical depth reduces pulses with a break energy of  $> 1$  MeV. If the Lorentz factor distribution has multiple peaks, the distribution of the break energy can be consistent with observations.

**Key words:** gamma rays: bursts—radiation mechanisms: non-thermal—shock waves

## 1. Introduction

Gamma-ray bursts (GRBs) are short ( $\lesssim 10$  s) bursts of low-energy  $\gamma$ -rays. One of the most important characteristics of the GRB spectra is the existence of a typical break energy scale. The observed spectra of GRBs are approximated by a broken power law and the photon number spectra are approximated as  $\sim \varepsilon^{-2}$  above the break energy and  $\sim \varepsilon^{-1}$  below that. The

standard scenario for producing GRBs is the dissipation of the kinetic energy of a relativistic flow by relativistic shocks (see, e.g., a review by Piran 1999). The rapid time variabilities observed require that the GRB itself must arise from internal shocks within the flow. The radiation is emitted by relativistic electrons in the shocked region. The observations are well-described by synchrotron emission (Cohen et al. 1997; Wijers, Galama 1999). Kobayashi et al. (1997) shows that the internal shock can reproduce the temporal structure of GRBs. A large fraction of the kinetic energy could be converted to radiation by the internal shocks (Kobayashi, Sari 2001).

The internal shock model is roughly represented by colliding shells. The collisions are considered to occur within a wide range of radius  $r$ . The energy efficiency argument requires a large dispersion of the initial Lorentz factor  $\Gamma$  (Kobayashi, Sari 2001; Beloborodov 2000). In spite of the large dispersions of  $r$  and  $\Gamma$  in the model, the apparent clustering of the break energy of the GRB spectra in the 50 keV–1 MeV range is reported in the BATSE observation (Preece et al. 2000). It is strange that pulses in a burst tend to have similar break energies. The break energy distribution is in agreement with a log-normal distribution. This distribution seems to suggest small dispersions of  $r$  or  $\Gamma$ .

In this paper, based on numerical simulations, we examine whether the standard internal shock model can reproduce the narrow distribution of the break energy. Guetta et al. (2001) showed that the internal shock model can reproduce the typical break energy. However, the dispersion of the break energy has not been explained so far. In our simulation, as Guetta et al. (2001) did, we include the effect of the Thomson optical depth due to  $e^\pm$  pairs produced by synchrotron photons. We treat the pair optical depth more precisely. In addition, our improvements in the numerical simulations over those in Guetta et al. (2001) take into account shell splitting and the spectral energy band in the observation. From our simulation we obtain some restrictions on GRB models. In section 2 we explain our simulation method. In section 3 the numerical results are given. In section 4 we summarize our results.

## 2. Method of Simulation

In order to examine the distribution of the break energy, we consider a spherical wind consisting of  $N$  shells. Each shell is characterized by the Lorentz factor  $\Gamma_i$ , mass  $M_i$ , width  $W_i$ , and radius from the center  $r_i$ . Following the evolution of the shells, there will be numerous collisions between different shells. For each collision we calculate the break energy, optical depth, and flux. In order to simplify our model we idealize the situation. Some approximations are adopted in our formulation, as discussed below.

### 2.1. Break Energy

In this subsection we explain our method to obtain the break energy. Let us consider

shells with different Lorentz factors,  $x \equiv \Gamma_r/\Gamma_s > 1$ . The relative Lorentz factor is  $\Gamma_{\text{rel}} \sim (x + 1/x)/2$ . The rapid and slower shells are denoted by subscripts r and s, respectively. We assume that the widths of the shells are comparable in the interstellar medium (ISM) rest frame as  $W_i = W$ . Under these assumptions, we can obtain the ratio of the baryon number density,  $n_r/n_s$ . For equal mass shells ( $M_i = \text{const.}$ )  $n_r/n_s = 1/x$ , while  $n_r/n_s = 1/x^2$  for equal energy shells ( $M_i\Gamma_i = \text{const.}$ ). In this paper,  $n$  and internal energy density  $e$  are measured in the fluids' rest frame.

When the rapid shell catches up with the slower one at some radius  $r$ , the forward and reverse shocks form. The shock conditions and the equality of pressures along the contact discontinuity (Sari, Piran 1995) yield

$$\frac{(\Gamma_F - 1)(4\Gamma_F + 3)}{(\Gamma_R - 1)(4\Gamma_R + 3)} = \frac{n_r}{n_s}, \quad (1)$$

where  $\Gamma_F$  and  $\Gamma_R$  are the Lorentz factors of the relative motion between the regions separated by the forward shock and by the reverse shock, respectively. The equality of the velocities along the contact discontinuity gives  $\Gamma_R = \Gamma_F\Gamma_{\text{rel}} - \sqrt{(\Gamma_F^2 - 1)(\Gamma_{\text{rel}}^2 - 1)}$ . In the case of equal mass shells or equal energy shells, the solution for  $\Gamma_R$  depends on only the ratio of the Lorentz factors  $x$ . The internal energy density in the shocked regions is given by

$$e = \frac{(\Gamma_R - 1)(4\Gamma_R + 3)M_r c^2}{4\pi r^2 \Gamma_r W}, \quad (2)$$

where  $M_r$  is the mass of the rapid shell.

We now consider the synchrotron emission from shocked shells. Since a rapid shell has a larger energy and a lower number density in the cases of equal mass and equal energy, the average energy per one electron in the reverse shock is larger than that in the forward shock. The reverse shock emission is more luminous and harder than the forward shock emission. Therefore, we consider only the emission from the reverse shock. The shock is assumed to accelerate electrons in the shell material into a power-law distribution,  $N(\gamma_e) \propto \gamma_e^{-p} (\gamma_e \geq \gamma_{e,\text{min}})$ . Assuming that constant fractions,  $\epsilon_B$  and  $\epsilon_e$ , of the internal energy go into the magnetic field and the electrons, respectively, one finds that the magnetic field and the typical random Lorentz factor of electrons are given by  $B^2 \propto \epsilon_B e$  and  $\gamma_{e,\text{min}} \propto \epsilon_e (\Gamma_R - 1)$ , respectively.

The synchrotron process is a very efficient radiation process. With the strong magnetic field required to produce the observed gamma-ray, the synchrotron cooling time is very short compared to the dynamical time of the shock. In this fast cooling case (Sari et al. 1998), the photon number density distribution at the fluid rest frame is given by

$$\frac{dn_\gamma(\varepsilon)}{d\varepsilon} = \frac{p-2}{2p-2} \frac{\epsilon_e e}{\varepsilon_p^2} \cdot \begin{cases} (\varepsilon/\varepsilon_p)^{-3/2} & \text{for } \varepsilon < \varepsilon_p, \\ (\varepsilon/\varepsilon_p)^{-(p+2)/2} & \text{for } \varepsilon \geq \varepsilon_p, \end{cases} \quad (3)$$

where the break energy  $\varepsilon_p$  is the typical energy of synchrotron photons emitted by electrons of  $\gamma_{e,\text{min}}$ . Since the shocked fluid is moving with the Lorentz factor,  $\Gamma_m \sim \Gamma_r(\Gamma_R - \sqrt{\Gamma_R^2 - 1})$ , the observed break photon energy is

$$\varepsilon_p^{\text{obs}} = 610 \epsilon_e^2 F(x) \Gamma_{s,2} \sqrt{\Sigma/\Delta} \text{ keV}, \quad (4)$$

where  $F(x) = x^{1/2}(\Gamma_R - 1)^{5/2}(4\Gamma_R + 3)^{1/2}(\Gamma_R - \sqrt{\Gamma_R^2 - 1})$ . It behaves as  $\sim x^2/4$  at  $x \gg 1$ . We have scaled the parameters as  $\epsilon_{B,-1} = \epsilon_B/0.1$ ,  $M_{48} = M_{\text{r}}c^2/10^{48}$  ergs,  $r_{13} = r/10^{13}$  cm,  $W_7 = W/10^7$  cm, and  $\Gamma_{s,2} = \Gamma_s/100$ . We adopt  $p = 2.5$  here and hereafter. Since some parameters appear in the following formulae in the same combinations, we have defined two variables, a surface density  $\Sigma = M_{48}/r_{13}^2$  and an effective comoving shell width  $\Delta = W_7\Gamma_{s,2}/\epsilon_{B,-1}$  for convenience. In our simulation we neglect the effect of the cosmological redshift on the break energy.

## 2.2. Optical Depth Due to $e^\pm$ Pairs

Shells are initially optically thick due to Thomson scattering by electrons associated with baryons in the shell. For a large optical depth  $\tau$ , the radiative cooling time can be estimated as  $\sim \tau l/c$ , where  $l = W\Gamma_r/(4\Gamma_R + 3)$  is the shell width in the comoving frame. Comparing this with the cooling time due to the shell spreading  $\sim l/c$ , the radiated energy is negligible for  $\tau \gg 1$ . Then, all of the internal energy is transformed back to kinetic energy (Kobayashi, Sari 2001). Thus, we could not observe the emission from it, until it comes from outside of the photosphere, where the optical depth  $\tau_T = 2\sigma_T M/4\pi r^2 m_p \sim 0.7\Sigma$  becomes unity. This is a well-know result, but the estimate may undergo a significant change in the internal shock model if we take into account  $e^\pm$  pairs produced by the synchrotron photons (Guetta et al. 2001). In the fluid rest frame, the break photon energy  $\varepsilon_p$  is much smaller than the electron mass. However, the photon distribution extends to high-energy as a power law. The pairs caused by the high energy photons may contribute significantly to the optical depth.

When a photon of energy  $\varepsilon$  interacts with a photon of  $\varepsilon'$  at an incident angle  $\theta$ , the cross section of the pair creation is written as  $\sigma_\pm = \sigma_T f(y)$  (Berestetskii et al. 1982), where

$$f(y) = \frac{3}{16}(1 - y^2) \left[ (3 - y^4) \ln \frac{1 + y}{1 - y} - 2y(2 - y^2) \right]. \quad (5)$$

The dimensionless value  $y$  is defined by  $y^2 = 1 - (2m_e^2 c^4)/[\varepsilon\varepsilon'(1 - \cos\theta)]$ . The optical depth to pair-creation is given by

$$\tau_{\gamma\gamma}(\varepsilon) = \int (1 - \cos\theta) d\Omega \int_{\frac{2m_e^2 c^4}{\varepsilon(1 - \cos\theta)}}^{\infty} d\varepsilon' \frac{dn_\gamma(\varepsilon')}{d\varepsilon' d\Omega} \sigma_{\gamma\gamma}(\varepsilon', \varepsilon) l \quad (6)$$

$$= \sigma_T l \frac{4(p-2)}{(p-1)(p+4)} \frac{\epsilon_e e}{\varepsilon_p} \left( \frac{\varepsilon\varepsilon_p}{m_e^2 c^4} \right)^{p/2} C(p), \quad (7)$$

where

$$C(p) \equiv \int_0^1 dy (1 - y^2)^{p/2-1} y f(y). \quad (8)$$

The value of  $C(p)$  is not sensitive to  $p$ , and  $C(2.5) \sim 0.075$ . Since we use the power-law distribution  $dn_\gamma/d\varepsilon \propto \varepsilon^{-(p+2)/2}$  in the integration, the optical depth is overestimated for photons with high energy  $\varepsilon \gtrsim 2m_e^2 c^4/\varepsilon_p$ , which interact with photons mainly in the low-energy portion

$dn_\gamma/d\varepsilon \propto \varepsilon^{-3/2}$ . However, the exact value is not important for the high-energy photons when we estimate the number of  $e^\pm$  pairs below, because the corrected optical depth is also large enough to annihilate all of them. For  $p = 2.5$  we obtain

$$\tau_{\gamma\gamma}(\varepsilon) = 3.3 \epsilon_e^{3/2} G(x) \Sigma^{9/8} \Delta^{-1/8} (\varepsilon/m_e c^2)^{5/4}, \quad (9)$$

where  $G(x) = (\Gamma_R - 1)^{13/8} (4\Gamma_R + 3)^{1/8} / x^{1/8}$ . Although the optical depth to pair-creation for photons with the typical energy of  $\varepsilon_p \ll m_e c^2$  is very small, it does not necessarily imply that the number of  $e^\pm$  pairs is negligible for Thomson scattering. Considering that photons with energy  $\varepsilon$  interact mainly with those with energy  $\sim 2m_e^2 c^4 / \varepsilon$  to produce pairs, we can estimate the optical depth due to the pairs as

$$\tau_\pm \sim 2\sigma_T l \int_{\sqrt{2}m_e c^2}^{\infty} d\varepsilon \frac{dn_\gamma(\varepsilon)}{d\varepsilon} (1 - e^{-\tau_{\gamma\gamma}}). \quad (10)$$

If we consider only the effect by the electrons accompanied by baryons, the expanding ejecta becomes optically thin when the surface density  $\Sigma \propto r^{-2}$  decreases down to  $\sim 1$ . However, the  $e^\pm$  pairs produced by the synchrotron photons generally increase the optical depth significantly. Then, the ejecta is required to expand beyond  $\Sigma \sim 1$  to radiate. In figure 1 we plot the value of the surface density  $\Sigma_M$ , at which the ejecta becomes optically thin, as a function of  $x$ . In order to plot figure 1, we have numerically solved equation (1) and integrated equation (10). If we describe the system as an inelastic collision between two masses, and half of the internal energy is converted to pairs as Guetta et al. (2001) assumed,  $\Sigma_M$  is estimated to be  $\sim 0.017\epsilon_e^{-1}\sqrt{x}/(1+x-2\sqrt{x})$ . This approximation generally gives a smaller value.

Since the break energy  $\varepsilon_p^{\text{obs}}$  is proportional to  $\Sigma^{1/2}$ , a collision occurring with larger  $\Sigma$  radiates harder photons. Then, the hardest synchrotron photons are emitted just above the radius where  $\Sigma = \Sigma_M$  for given values of the parameters  $x$ ,  $\Delta$ , and  $\Gamma_s$ . We define the maximum break energy  $E_M$  as the break energy emitted from the radius where  $\Sigma = \Sigma_M$ . The value of  $E_M$  is obtained from equation (4) with  $\Sigma = \Sigma_M$ . Figure 2 depicts  $E_M$  as a function of  $x$ . We can see that the photon pair-creation effect makes  $E_M$  significantly smaller (solid lines) compared to the case without the effect (dotted lines). According to figure 2, it is difficult to obtain a break energy of more than 1 MeV for  $x \leq 20$ . The upper limit of the break energy is determined by the Thomson optical depth due to  $e^\pm$  pairs, and it is close to the typical observed break energy. This result agrees with Guetta et al. (2001).

In the parameter region of our interest, the critical photon energy  $\varepsilon_\tau$ , at which the optical depth  $\tau_{\gamma\gamma} = 1$ , is larger than  $\sqrt{2}m_e c^2$ . Then, we obtain the approximation,

$$\tau_\pm \sim 300\epsilon_e^3 G^2(x) \Sigma^{9/4} \Delta^{-1/4}, \quad (11)$$

where we neglect a logarithmic factor of  $\varepsilon_\tau$ . We adopt this approximation in our simulation.

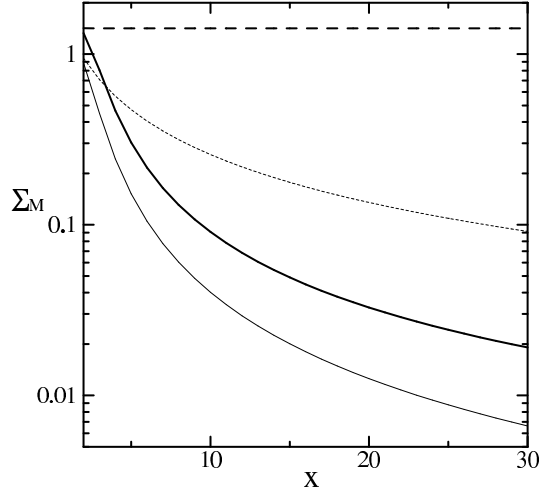


**Fig. 1.** Plot of  $\Sigma_M$  (solid line) against  $x$ . The thick and thin lines are for equal-mass and equal-energy cases, respectively. The dotted lines represent the values without pair-creation. For equal mass the value is constant as  $\Sigma_M = 1.4$ . Here, we assume  $\Delta = 1$  and  $\epsilon_e = 0.5$ .

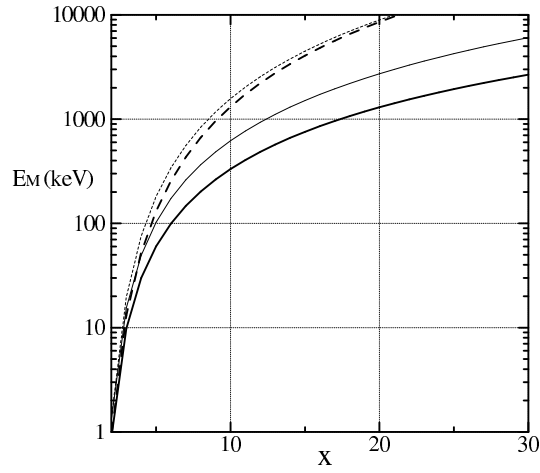


**Fig. 2.** Plot of  $E_M$  (solid line) against  $x$ . The dotted lines are values obtained without the process of pair-creation. The thick and thin lines are for equal-mass and equal-energy cases, respectively. Here, we assume  $\Delta = 1$ ,  $\epsilon_e = 0.5$ , and  $\Gamma_{s,2} = 1$ .

### 2.3. Sampling of Break Energy

Setting the initial distributions of the Lorentz factor  $\Gamma_i$  and separation between shells  $L_i$ , we follow the evolution of the shells until there are no more collisions, i.e., until the shells are ordered by increasing value of the Lorentz factors. For each collision, using equations (1), (4), and (11), we estimate the break energy and the optical depth due to electron–positron pairs. We approximate the radiation energy as

$$E_{\text{rad}} = \epsilon_e [M_r(\Gamma_r - \Gamma'_m) + M_s(\Gamma_s - \Gamma'_m)], \quad (12)$$

where

$$\Gamma'_m = \sqrt{\frac{M_r\Gamma_r + M_s\Gamma_s}{M_r/\Gamma_r + M_s/\Gamma_s}}, \quad (13)$$

as conventionally assumed (Kobayashi, Sari 2001). After a fraction  $\epsilon_e$  of the internal energy is emitted, the shells will split, transforming the remaining internal energy back to kinetic energy. In our simulation, the process of the shell splitting is basically the same as in Kobayashi, Sari (2001). The introduction of shell splitting in the simulation increases the number of collisions and the energy efficiency. In this paper, for simplicity, we assume that each mass and width of the shell are conserved before and after its collision. If  $\tau_{\pm} \geq 1$ , we force  $\epsilon_e = 0$ . Then the collisions of shells for  $\tau_{\pm} \geq 1$  are similar to the perfectly elastic collisions of pool balls.

In order to include the effect of the spectral energy band in observations, we produce pseudo observational data from our simulation. Using the spectrum of equation (3), we estimate the flux between 20 and 2000 keV from the radiation energy and break energy. We neglect the effect of the spectral sensitivity in BATSE instruments. The effective area changes only by a factor of two in most parts of the spectral energy band, so that the effect of the sensitivity can be negligible. From the estimated flux we write light curves by the same method as in Kobayashi et al. (1997). The light curves are superpositions of many pulses emitted from all collisions. The light curve peaks are identified with the peak-finding algorithm described by Li, Fenimore (1996). A peak time  $T_p$  is identified, if the peak photon flux  $C_p$ , photon fluxes  $C_1$  ( $T_1 < T_p$ ), and  $C_2$  ( $T_2 > T_p$ ) satisfy  $C_p - C_{1,2} > N_{\text{var}}\sqrt{C_p}$  and there are no time bins between  $T_1$  and  $T_2$  with photon flux higher than  $C_p$ . We adopt  $N_{\text{var}} = 0.3$ . The results do not strongly depend on  $N_{\text{var}}$  (Spada et al. 2000). Each peak is identified as an “observable pulse” in our simulation. The light curve valleys are identified as the minima between two consecutive peaks. We divide the light curves in time into some regions by valleys and identify them as the observed duration time of each pulse. One observable pulse may be the composition of multiple pulses emitted from different collisions. For each temporal region, by attaching a fluence weight, we average the break energies of all pulses arrived during the period. We adopt the average break energy as the “observable break energy” for each temporal region. This treatment is different from the method used in an actual observation. In our simulation, however, one pulse greatly overwhelms other dim pulses in most cases. Therefore, our method is harmless when

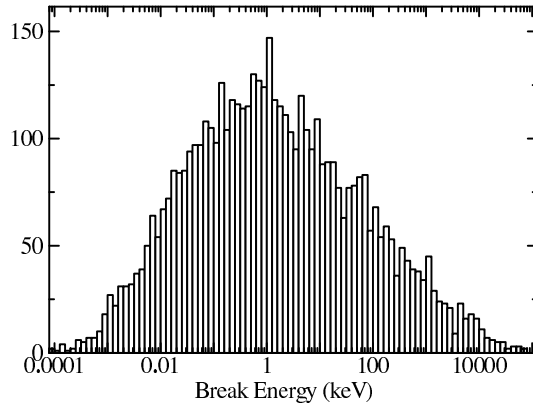


**Fig. 3.** Distribution of the break energy for all collisions. The effect of the Thomson optical depth is neglected.

determining the break energy.

### 3. Results of Simulation

#### 3.1. Continuous $\Gamma$ -Distribution

In our simulation, the initial shells are assumed to have equal mass  $M$  and width  $W$ . The distributions of the initial Lorentz factor  $\Gamma_i$  of each shell and initial separation  $L_i$  between two consecutive shells are determined by the character of the central engine on which we have little information. In our simulation we assume that  $\Gamma_i$  is to be distributed uniformly in logarithmic space between  $\log\Gamma_m$  and  $\log\Gamma_M$  (the number distribution of shells is proportional to  $1/\Gamma$ ). The initial separation  $L_i$  is also assumed to distribute in the same way between  $\log W$  and  $\log L_M$ . We perform 100 simulations with  $N = 50$ ,  $\Gamma_m = 30$ ,  $\Gamma_M = 3000$ ,  $W/c = 10^{-2}$  s,  $L_M/c = 1$  s,  $\epsilon_e = 0.6$ ,  $\epsilon_B = 0.1$ , and a total initial kinetic energy of  $E_{\text{iso}} = 10^{52}$  erg. First we present the results, neglecting the effect of  $\tau_{\pm}$ . Figure 3 shows a histogram of the break energy for all collisions, neglecting the spectral band in the observation. The break energies widely distribute from the optical range to 10 MeV. This result apparently contradicts the observation. We then take into account the Thomson optical depth. As is shown in figure 4, the break energies above  $\sim 1$  MeV are suppressed, as we have speculated in subsection 2.2. However, there remain many pulses with a low break energy. The effect of the Thomson optical depth reduces only high-break pulses.

However, we can not observe all of the pulses emitted from all collisions. A dimmer pulse may be overwhelmed by other brighter pulses. Since a dimmer pulse is expected to have a lower break energy, actual observations reduce the number of pulses with a low break energy. In addition, a large energy fraction of emission with a very low break energy may be out of the spectral energy band in the observation. Therefore, we mimic the BATSE observation by producing light curves from the simulations, as explained in subsection 2.3, and define the



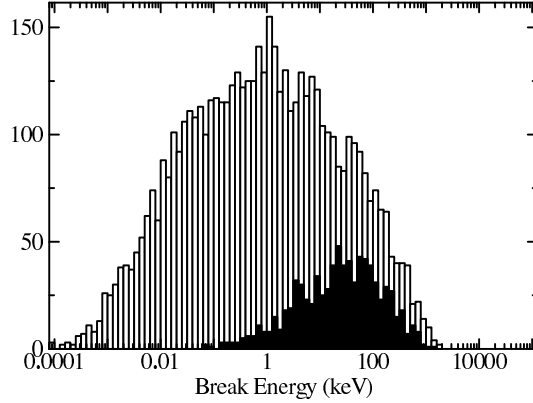


**Fig. 4.** Distribution of the break energy for all collisions (white) and observable pulses (black). The effect of the Thomson optical depth is  $t$

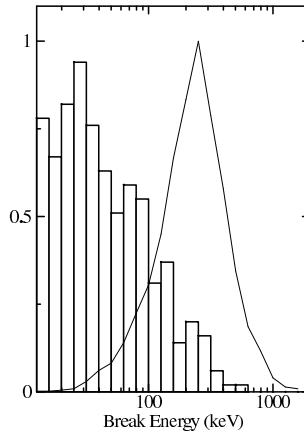


**Fig. 5.** Same as figure 4 for observable pulses. Here we include the cosmological redshift effect, assuming  $z = 1.5$ . The solid line is the BATSE observation. There are many other pulses outside of this energy band. They should be counted as pulses whose spectra have no break energy.

observable pulses and their break energies. In figure 4, we show the result obtained from the pseudo observational data. Samples with lower break energy diminish drastically. In figure 5 we magnify the result around the BATSE band. Although the peak of the distribution is around the lowest limit of the BATSE band, the dispersion is significantly larger than the observation. There are many pulses with a break energy of  $< 20$  keV, which should be observed as “no break” pulses. In the spectral energy band only high-energy tails of bright spectra of such pulses are detected, and they make significant peaks in the light curve.

Regarding the observable pulses in figures 6 and 7, we show the relations between the break energy and the collision radius  $r$ , and between the break energy and the ratio of the Lorentz factors  $x$ , respectively. The collision radius and ratio  $x$  are obtained averaging in the same way as the break energy. According to these figures, the break energy is mainly determined by the ratio  $x$  rather than  $r$ . Collisions with a smaller  $x$  produce lower break energies, which

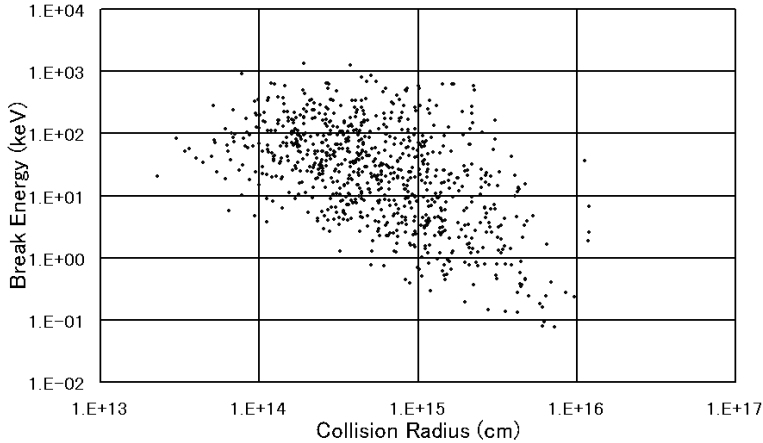


Fig. 6. Relation between the break energy and collision radius.

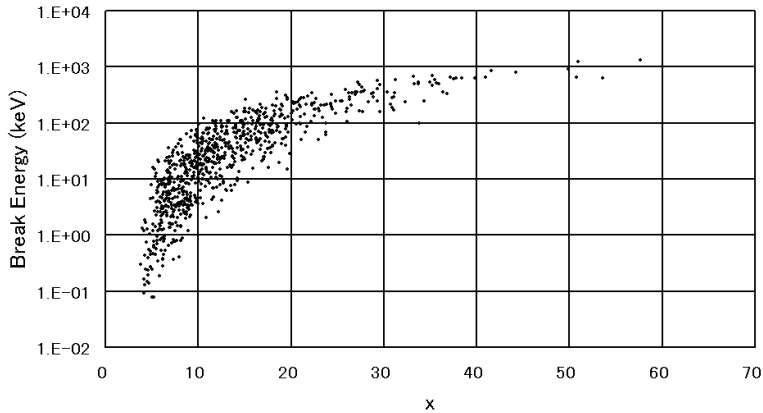


Fig. 7. Relation between the break energy and the ratio  $x$ .

cause a large dispersion of the break energy. The lower limit of the collision radius in figure 6 is determined by the Thomson optical depth.

In this model, the fraction of the emission energy to the total kinetic energy is  $16.9 \pm 2.0\%$ . As Kobayashi, Sari (2001) claimed, the introduction of shell splitting increases the energy efficiency compared with that of Guetta et al. (2001) (typically a few percent). In the pseudo BATSE band, the energy efficiency is  $2.9 \pm 0.9\%$ . About four-times radiation energy in the BATSE band is emitted outside of the BATSE band.

### 3.2. Bimodal $\Gamma$ -Distribution

We have simulated for other types of distributions of  $\Gamma$ . However, as long as the  $\Gamma$ -distribution is continuous and has only one peak, the results do not change basically. The models predict many “no break” pulses. Let us consider a  $\Gamma$ -distribution that has a maximum at  $\Gamma = \Gamma_p$ . If we randomly choose two shells in this distribution, the most probable  $\Gamma$ s of two shells are around  $\Gamma_p$ . Therefore, we cannot avoid numerous collisions with  $x \sim 1$ , which leads to low break energies. Of course, a too small  $x$  leads to too dim emission. However, emission

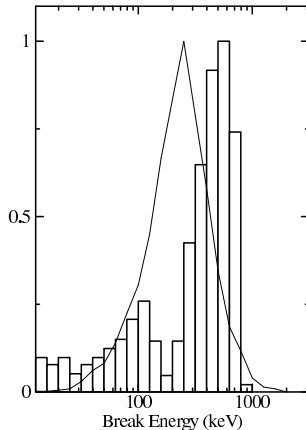


**Fig. 8.** Distribution of the observable break energy for the bimodal distribution. The effect of the Thomson optical depth is taken into account. Here, we include the cosmological redshift effect assuming  $z = 1.5$ . The solid line is the BATSE observation.

from a marginal value of  $x$  ( $\sim 5$ ) is luminous enough in spite of the small break energy.

If the  $\Gamma$ -distribution has two peaks, the probability function of  $x$  may have a maximum at  $x \gg 1$ . As one example, we make a simulation for a bimodal  $\Gamma$ -distribution: one half of the shells have  $\Gamma = 30$  and the other half have  $\Gamma = 3000$  initially. The parameters are common to those described in the former subsection. The result is shown in figure 8. Since collisions with  $\Gamma = 30$  and  $\Gamma = 3000$  are dominant events in this case, break energies distribute narrowly. The dispersion of the break energy is consistent with the observation. It is trivial that we can adjust the peak of the distribution to the observation more closely by changing the parameter  $\epsilon_e$ .

The fraction of the emission energy to the total kinetic energy is  $65.1 \pm 6.6\%$ . In the pseudo BATSE band, the energy efficiency is  $18.7 \pm 2.5\%$ . The bimodal distribution is advantageous to the energy efficiency too.

#### 4. Conclusions and Discussion

Following the standard scenario of GRB, we simulate internal shocks, including the effects of shell splitting and the Thomson optical depth due to electron–positron pairs produced by synchrotron photons. We produce pseudo observational data and estimate the break energy. The effect of the Thomson optical depth reduces the pulses with a break energy of  $> 1$  MeV, which is consistent with Guetta et al. (2001). The shell-splitting effect increases the energy efficiency. However, many “no break” pulses should be observed in the case of a one-peak, continuous  $\Gamma$ -distribution. Even if we alter some assumptions (shell splitting, equal shell mass, etc.) in our model, the qualitative result is basically the same. Within our simple method, “no break” pulses are unavoidable, though we take into account the spectral energy band in the observation. Collisions with a small ratio  $x$  cause “no break” pulses. Preece et al. (2000) insists that the small dispersion of the break energy is not due to the observational selection

effects. However, we should henceforth consider the possibility of selection effects on the BATSE observation.

The  $\Gamma$ -distribution is determined by the character of the central engine. If the initial  $\Gamma$ -distribution is discrete, or has multiple peaks, like the bimodal distribution, the distribution of the break energy can be consistent with the observation. The bimodal distribution is favorable for the energy efficiency. However, we do not know if such a distribution is realistic or not.

Judging from figure 7, if we choose pulses emitted from collisions with  $x \gtrsim 10$ , most of the observable break energies are in the BATSE band. Therefore, if some microscopic processes prohibit collisions with  $x \lesssim 10$  from emitting photons, the small dispersion of the break energy can be reproduced. One of the candidates for such processes is in the electron acceleration mechanism, which is not well understood. In the standard GRB model, a large fraction of the kinetic energy carried by protons is efficiently converted into that of relativistic electrons in the shocked region. However, this premise has not been proven theoretically. It is apparent that the Coulomb interaction cannot transport the internal energy of heated protons into electrons to achieve energy equipartition, because the time scale of the Coulomb interaction is much longer than the dynamical time scale. In our model,  $x = 10$  corresponds to  $\Gamma_R = 2.57$ . Therefore, the threshold  $x \simeq 10$  is a border between mild-relativistic and ultra-relativistic shock. If the energy of protons can be efficiently transported into electrons only for ultra-relativistic shock, the distribution of the break energy can be explained. Hoshino, Shimada (2002) proposed a new acceleration mechanism: shock surfing acceleration. This mechanism effectively accelerates only electrons in the cases of a strong shock. Such a study might explain the break energy in the future.

We would like to thank T. Sakamoto for providing information about the BATSE instruments. We also thank R. Preece for useful discussions, as well as providing and helping with the some of the BATSE data. K.A. is supported by the Japan Society for the Promotion of Science. S.K. thanks support through the Center for Gravitational Wave Physics, which is funded by NSF under cooperative agreement PHY 01-14375.

## References

- Beloborodov, A. M. 2000, *ApJ*, 539, L25  
Berestetskii, V. B., Lifshitz, E. M., & Pitaevskii, L. P. 1982, *Quantum Electrodynamics* (New York: Pergamon), p. 371  
Cohen, E., Katz, J. I., Piran, T., Sari, R., Preece, R. D., & Band, D. L. 1997, *ApJ*, 488, 330  
Guetta, D., Spada, M., & Waxman, E. 2001, *ApJ*, 557, 399  
Hoshino, M., & Shimada, N. 2002, *ApJ*, 572, 880

- Kobayashi, S., Piran, T., & Sari, R. 1997, ApJ, 490, 92  
Kobayashi, S., & Sari, R. 2001, ApJ, 551, 934  
Li, H., & Fenimore, E. E. 1996, ApJ, 469, L115  
Piran, T. 1999, Phys. Rep., 314, 575  
Preece, R. D., Briggs, M. S., Mallozzi, R. S., Pendleton, G. N., Paciesas, W. S., & Band, D. L. 2000, ApJS, 126, 19  
Sari, R., & Piran, T. 1995, ApJ, 455, L143  
Sari, R., Piran, T., & Narayan, R. 1998, ApJ, 497, L17  
Spada, M., Panaitescu, A., & Mészáros, P. 2000, ApJ, 537, 824  
Wijers, R. A. M. J., & Galama, T. J. 1999, ApJ, 523, 177